Quasilocal entanglement across the Mott-Hubbard transition

note finali coverpage

(Article begins on next page)

22 May 2024

# Quasilocal entanglement across the Mott-Hubbard transition

Gabriele Bellomia,[1, *] Carlos Mejuto-Zaera,[1, †] Massimo Capone,[1, 2, ‡] and Adriano Amaricci[2, §]

[1]*International School for Advanced Studies (SISSA), Via Bonomea 265, 34136 Trieste, Italy*
[2]*Istituto Officina dei Materiali (CNR-IOM), Via Bonomea 265, 34136 Trieste, Italy*

The possibility to directly measure, in a cold-atom quantum simulator, the von Neumann entropy and mutual information between a site and its environment opens new perspectives on the characterization of the Mott-Hubbard metal-insulator transition, in the framework of quantum information theory. In this work we provide an alternative view of the Mott transition in the two-dimensional Hubbard model in terms of rigorous *quasilocal* measures of entanglement and correlation between two spatially separated electronic orbitals, with no contribution from their environment. A space-resolved analysis of cluster dynamical mean-field theory results elucidates the prominent role of the *nearest-neighbor* entanglement in probing Mott localization: both its lower and upper bounds sharply increase at the metal-insulator transition. The two-site entanglement *beyond nearest neighbors* is shown to be quickly damped as the inter-site distance is increased. These results ultimately resolve a conundrum of previous analyses based on the single-site von Neumann entropy, which has been found to monotonically decrease when the interaction is increased. The quasilocal two-site entanglement recovers instead the distinctive character of Mott insulators as strongly correlated quantum states, demonstrating its central role in the 2$d$ Hubbard model.

## I. INTRODUCTION

The Hubbard model is a cornerstone of condensed matter physics as the paradigmatic description of systems with strongly correlated electrons and, in its two-dimensional version, as a central building block to understand high-temperature superconductivity in copper oxides. Besides the investigation of the various landmarks of the cuprate phase diagram, like $d$-wave superconductivity, charge-ordering/stripes and pseudogap, a prominent role is played by the Mott metal-insulator transition (MIT), which is arguably the most direct signature of strong correlations [1, 2].

On the other hand, the flourishing of quantum information theory has greatly emphasized the possibility to quantify the entanglement of quantum many-body systems and its central role in the study of quantum phase transitions [3–6], topological order [7–9], chemical bonding [10–12] and the development of highly optimized numerical methods [13–15].

In the last few years we have seen the first efforts to revisit traditionally successful descriptions of the Mott-Hubbard transition in terms of this new approach. Initial studies within single-site dynamical mean-field theory (DMFT) [16] have attempted to probe the development of entanglement across the Mott transition [17]. The spatially local nature of the correlations in this framework makes it natural to use on-site markers like *single-site entanglement entropy* or *single-site mutual information*.

A similar approach has been more recently pursued [18–20] within cluster dynamical mean-field theory (CDMFT), which includes the effects of short-range spatial correlations within finite clusters [21–23] onto these single-site entropic measures.

The choice of these markers is driven by their direct experimental access in cold-atom experiments [24] but it is also justified *a priori* by the expectation that, at least in a paramagnetic Mott insulator without long-range order, the particles are essentially localized and the relevant correlation functions are expected to be short ranged. Yet, the evolution of the single-site entanglement entropy as a function of the interaction strength does not seem to convey the expected physical picture for a correlation-driven localization.

In fact, despite being clearly influenced by the Mott transition, this quantity decreases from the metallic to the insulating phase [17, 18]. This seems in sharp conflict with the intuitive notion that nearly localized Mott insulators are underpinned by the development of some kind of entanglement among electronic orbitals at different sites. We can connect this shortcoming with the fact that, regardless of the approximation, the single-site entanglement entropy in the half-filled one-band Hubbard model closely follows the behavior of the local double occupancy, which naturally decreases across the Mott transition [17]. At a more fundamental level, we notice that the single-site entanglement entropy results from contributions of any kind of nonlocal quantum correlations (bi/multipartite terms at different spatial ranges), and it does not directly reflect the specific behavior of any such term [25]. Remarkably, recent extensions of the analysis to multisite entanglement entropies [26, 27] have established the same qualitative picture, suggesting that nonlocal entanglement needs to be addressed carefully to uncover its role in Mott localization.

In this work we overcome these limitations by considering *quasilocal* measures of entanglement, namely the entanglement between two lattice sites at distances ranging from nearest-neighbors, playing a major role, to

more distant pairs. We compute these objects within zero-temperature CDMFT, using a combination of numerical methods: a Lanczos/Arnoldi exact diagonalization scheme [28, 29] and the recently introduced configuration-interaction based solver [30], which gives access to the larger clusters required to assess the entanglement beyond nearest neighbors. In order to identify the fundamental information related to the Mott transition we consider paramagnetic solutions in which magnetic ordering is inhibited, as it has been done also in the previous works where the connection between the MIT and entanglement estimators has been addressed [17–20].

We will adopt and discuss different quantities, focusing on the estimation of the orbital entanglement between lattice sites. We compute upper and lower bounds for the two-site entanglement, by using suitable correlation measures [12, 31] and physically motivated superselection rules on the relevant reduced density matrices [32, 33]. This allows us to obtain a terse physical picture of quantum and classical correlations across the Mott transition in the $2d$ Hubbard model, as well as a distinctive characterization of the metallic and insulating phases. In particular, we show that the nearest-neighbor entanglement of the Mott insulator is larger with respect to the Fermi liquid state, recovering the intuitive expectations for a strongly correlated electronic system.

The rest of this work is organized as follows. In Sec. II we will present the measures of quasilocal correlation and entanglement. We further discuss the selected superselection rules and elucidate their role in the construction of lower bounds to the two-site entanglement. In Sec. III we briefly introduce the model and the CDMFT solvers used to approximate its solution. In addition we discuss the evaluation of single- and two-site reduced density matrices within the chosen numerical schemes. In Sec. IV we present and discuss our results about the evolution of correlations and entanglement across the Mott transition. Section V contains a discussion on the robustness of the single- and two-site measures of entanglement with respect to the superselection rules, in the two phases of the model. In Sec. VI we draw conclusions and outline some future perspectives. Finally, in Appendix A we give further details on the implementation of the superselected measures of correlation and entanglement, in Appendix B we outline the derivation of a sum rule for the two-site mutual information, in Appendix C we summarize in a table the properties of the entanglement and correlation markers used in this work and in Appendix D we provide additional details on the numerical calculations.

## II. ENTANGLEMENT MEASURES

The key quantity for our analysis is the quasilocal orbital entanglement, as measured by the relative entropy of entanglement (REE) [34]. The relationships be-

tween the REE and different measures of entanglement, *e.g.* entanglement of formation, entanglement of distillation, etc. are extensively discussed in Refs. [12, 34].

In the following, we mostly deal with the case of bipartite entanglement between two spatially separated electronic orbitals. Thus, in order to formally define the corresponding REE, we consider two sites, not necessarily neighbors, as a subsystem of a full lattice. This subsystem can be further partitioned into the two distinct sites. The REE between these two sites corresponds to a minimal "distance" (quantum relative entropy) between the given two-site density matrix and the convex set of two-site states that are separable with respect to the bipartition [34]. In the following we will refer to this quantity as the two-site entanglement $E_{ij}$. Since there is not a simple parametrization for this convex set, a closed expression for the $E_{ij}$ remains elusive [35]. Yet, different bounds can be constructed via conventional quantities [12, 31] and suitable superselection rules [32, 33]. In the following we describe the evaluation of these quantities in terms of the ground state reduced density matrices for single- and two-site subsystems, as computed or measured within any theoretical or experimental method. We defer to Sec. III all the details specific to our numerical approach.

### A. Single- and two-site entanglement entropies

Let us consider the ground state density matrix $\rho_{\mathrm{gs}}$ for a lattice $\mathcal{L}$. The reduced density matrix (RDM) for a subsystem A of the lattice $\mathcal{L}$ reads

$$\rho_{\mathrm{A}} = \mathrm{Tr}_{j \in \mathcal{L} \backslash \mathrm{A}} \left( \rho_{\mathrm{gs}} \right) . \tag{1}$$

Given a single site $i$, we call local entanglement entropy the von Neumann entropy of $\rho_i$ [17–20, 25]

$$s_i = - \mathrm{Tr}(\rho_i \log \rho_i) \tag{2}$$

If $\rho_{\mathrm{gs}}$ describes a pure state then $s_i$ gives a well-defined measure of the bipartite entanglement between the single site and the surrounding lattice [25]. We stress that being one of the entangled parties a macroscopic subsystem, this quantity includes quantum correlations for all the spatial ranges encoded in the model, hence the name "local entanglement entropy" can be misleading.

In a similar way, we define a two-site entanglement entropy from the RDM of a pair of sites $\rho_{ij}$ as

$$s_{ij} = - \mathrm{Tr}(\rho_{ij} \log \rho_{ij}). \tag{3}$$

We indicate the particular case of nearest neighbors with the symbol $s_{\langle ij \rangle}$. The two-site entanglement entropy $s_{ij}$ shares most properties with $s_i$, being it a measure of the entanglement between a pair of sites and, again, their whole environment.

### B. Two-site mutual information (total correlation)

Given the entanglement entropies $s_i$ and $s_{ij}$, respectively of a single- and a two-site subsystem, we can define the mutual information between the two sites as [25]

$$I_{ij} = s_i + s_j - s_{ij}, \qquad (4)$$

reserving the symbol $I_{\langle ij \rangle}$ for the case of nearest neighbors.

The mutual information $I_{ij}$ gives a measure of all quantum and classical correlations between sites $i$ and $j$. To elucidate this, let us consider the density matrix of a generic bipartite quantum system $\rho_{AB}$, with $\rho_A$ and $\rho_B$ the reduced density matrices for an arbitrary pair of subsystems. The mutual information $I_{AB} = s_A + s_B - s_{AB}$, satisfies the following inequality [31]

$$I_{AB} \geq \frac{\left( \langle \mathcal{O}_A \otimes \mathcal{O}_B \rangle_{\rho_{AB}} - \langle \mathcal{O}_A \rangle_{\rho_A} \langle \mathcal{O}_B \rangle_{\rho_B} \right)^2}{2 \|\mathcal{O}_A\|^2 \|\mathcal{O}_B\|^2} \qquad (5)$$

where $\mathcal{O}_A$ and $\mathcal{O}_B$ are generic operators acting on the Hilbert spaces of subsystems A and B, respectively. If the composite system is pure ($s_{AB} = 0$), we have $I_{AB} = s_A + s_B = 2 s_A$. Because there is no classical correlation in a pure state, the mutual information between A and B measures only the quantum correlation between the two. If $s_{AB} \neq 0$ then $\rho_{AB}$ is a statistical mixture and $I_{AB}$ also includes classical correlations between A and B. Hence, $I_{AB}$ provides an upper bound to correlation functions for any pair of subsystem operators, namely it quantifies the maximum correlation between subsystems A and B.

### C. Entanglement bounds and superselection rules

Since a closed mathematical expression for the two-site entanglement, as measured by the REE, is inaccessible we aim at obtaining upper and lower bounds to $E_{ij}$. As for the two-site entanglement entropy and mutual information, we will notate the case of nearest neighbors with the symbol $E_{\langle ij \rangle}$.

As discussed above, the total correlation $I_{ij}$ includes different sources of correlations. Hence it provides a straightforward upper bound to the two-site entanglement $E_{ij} \leq I_{ij}$ [12, 25, 34]. A lower bound can be obtained by restricting the family of subsystem density matrices over which the distance in the definition of the REE is evaluated [32]. This restriction can be motivated by assuming suitable *local* superselection rules (SSR), which are generalizations of conventional selection rules, constraining the coherent superposition of states pertaining to different eigenvalues of selected local operators [32, 33]. The relevance of local SSR in the definition of physically accessible entanglement [33, 36–45] has been recently challenged by new arguments in quantum thermodynamics [46]. Notwithstanding their possible interpretation, it

has been shown that the SSR allow the definition of rigorous lower bounds to the two-site REE [32].

In the following, we consider particle number (N-SSR) and parity (P-SSR) superselection rules, corresponding to a restriction on the physical operations allowed on the electronic system, namely they must conserve either the local number of electrons $N_i$ or its parity. Using these SSR we obtain the following bounds for the two-site entanglement:

$$E_{ij}^{\text{N-SSR}} \leq E_{ij}^{\text{P-SSR}} \leq E_{ij}. \qquad (6)$$

Explicit expressions for $E_{ij}^{\text{N-SSR}}$ and $E_{ij}^{\text{P-SSR}}$ in terms of the components of the two-site reduced density matrices are reported in Appendix A.

It is important to observe that the N-SSR and P-SSR can also be applied to the local entanglement and the two-site total correlation, providing lower bounds to their magnitudes [47]

$$E_i^{\text{N-SSR}} \leq E_i^{\text{P-SSR}} \leq E_i \qquad (7)$$

$$I_{ij}^{\text{N-SSR}} \leq I_{ij}^{\text{P-SSR}} \leq I_{ij} \qquad (8)$$

A self-contained presentation of explicit expressions for these quantities is given in Appendix A. Here, we denote with $E_i^{\text{N(P)-SSR}}$ the superselected measure of the entanglement between a single site and the rest of the lattice. Note that this quantity does not in general correspond to the superselected local entanglement entropy as the ground state density matrix of the lattice cannot be guaranteed to be pure under the SSR [47], hence

$$E_i^{\text{N(P)-SSR}} \neq s_i^{\text{N(P)-SSR}}.$$

See Appendix A for an extended discussion.

Finally, we introduce the *superselection factors*

$$\xi_{E_i}^{\text{N(P)-SSR}} \overset{\text{def}}{=} \frac{E_i}{E_i^{\text{N(P)-SSR}}} \geq 1 \qquad (9)$$

$$\xi_{I_{ij}}^{\text{N(P)-SSR}} \overset{\text{def}}{=} \frac{I_{ij}}{I_{ij}^{\text{N(P)-SSR}}} \geq 1 \qquad (10)$$

in order to quantify the robustness of these entanglement and correlation measures, with respect to the two selected local superselection rules: the closer these factors are to the unity, the less relevant the superselection rules become in defining the corresponding measure.

## III. MODEL AND METHODS

We consider a single-band Hubbard model on the two-dimensional square lattice $\mathcal{L}$, with Hamiltonian

$$H = -t \sum_{\sigma} \sum_{\langle ij \rangle \in \mathcal{L}} \left( c_{i\sigma}^{\dagger} c_{j\sigma} + \text{h.c.} \right) + U \sum_{i \in \mathcal{L}} n_{i\uparrow} n_{i\downarrow} \qquad (11)$$

where $c_{i\sigma}$ ($c_{i\sigma}^{\dagger}$) is the annihilation (creation) operator of an electron with spin $\sigma$ at the site $i$ of the lattice, $n_{i\sigma} = c_{i\sigma}^{\dagger}c_{i\sigma}$ is the local spin density, $t$ is the nearest-neighbor hopping amplitude and $U$ is the local electronic interaction strength. In the following, we consider the regime of zero temperature and an occupation of one electron per site (half-filling). We set our unit of energy as the noninteracting half-bandwidth $D = 4t = 1$.

We solve this model using cluster dynamical mean-field theory (CDMFT) [16, 21–23]. This is a powerful non-perturbative tool to investigate the physics of strongly correlated electrons on a lattice, capturing local as well as nonlocal (short-range) correlations. The CDMFT solution maps the original lattice problem to a quasilocal embedding of a cluster of $N_{\mathrm{imp}}$ correlated sites into a noninteracting bath, which is self-consistently determined by the requirement that the Green's functions connecting sites within the cluster are the same as in the original lattice. This effective theory can be seen as a generalization of a quantum impurity model, hence we will refer to the $N_{\mathrm{imp}}$ cluster sites as impurity sites in the following.

In this work, we rely on a combined numerical analysis using two different methods to solve the quantum impurity cluster problem, namely Lanczos/Arnoldi exact diagonalization (ED) and adaptive sampling configuration interaction (ASCI). Both methods parametrize the noninteracting bath in terms of a finite number of sites, employing different algorithms to obtain the lower part of the energy spectrum and dynamical correlation functions. Given the unfavorable scaling of the computational effort with the number of impurity sites, the size of the clusters is severely limited allowing for a reliable estimate only of short-ranged spatial correlations.

Our ED solver leverages on the massively parallel implementation of Ref. [29], straightforwardly generalized to cluster methods [48]. To reduce the number of variables to be optimized, we employ a representation of the bath in terms of non-interacting *replicas* of the correlated cluster, diagonally coupled to the corresponding impurity sites [49, 50]. Their internal parameters, corresponding to on-site energies and nearest-neighbor hoppings are optimized through the self-consistency procedure, together with the impurity-bath hybridization amplitudes [29]. Thus a given number $N_{\mathrm{repl}}$ of replicas corresponds to $N_{\mathrm{bath}} = N_{\mathrm{imp}}N_{\mathrm{repl}}$ bath sites. In the following, we use ED to study $N_{\mathrm{imp}} = 1 \times 2$ and $N_{\mathrm{imp}} = 2 \times 2$ clusters, keeping a fixed total number of sites $N_{\mathrm{s}} = N_{\mathrm{imp}} + N_{\mathrm{bath}} = N_{\mathrm{imp}}(1 + N_{\mathrm{repl}}) = 12$.

In addition we employ the recently introduced ASCI solver for CDMFT [30, 51–53] to benchmark our results and study larger cluster sizes with respect to those accessible with the ED algorithm. This method provides a powerful algorithm [54, 55] capable of alleviating the ED limitations related to the exponential growth of the Hilbert space of the impurity problem: the ASCI Ansatz corresponds to an adaptively optimized truncation of the full impurity model Hilbert space in terms of a subset of selected Slater determinants, which together reconstruct

the majority of the ground state wave function. It further relies on optimizing an orbital active space by constructing a suitable natural basis from an approximated one-body RDM for the bath orbitals [30, 51, 53]. This results in a highly compact and accurate representation of the ground state [56] and of the one-body Green's functions [30], while reducing the overall computational cost.

Within the ASCI method the bath sites are split into groups of $N_{\mathrm{imp}}$ degenerate levels, with an all-to-all amplitude to the cluster impurity sites. The bath parameters are self-consistently determined by means of a recently introduced conic optimizer [57]. In this work we perform ASCI calculations addressing $N \times 2$ clusters sizes, with $N = 1, \ldots, 4$. We fix the number of bath sites to six times the number of cluster impurity levels which, using the bath degeneracy structure in Ref. [57], means that we have six nondegenerate bath energies.

The two methods, ED and ASCI, grant us direct access to an explicit representation of the ground state of the cluster impurity model. Using this information, we can build the zero temperature RDM for any cluster subsystem (*e.g.* two sites) using an on-the-fly trace over the bath and complementary impurity degrees of freedom. The local RDM, thoroughly studied in Refs. [17–20], is obtained by further tracing over all but one site.

Remarkably, we observe that a recent work by Roósz *et al.* [58] provides a recipe to obtain single-orbital and two-orbital RDM from the knowledge of single-particle and two-particle Green's functions alone, giving access to quasilocal entanglement and correlation measures to a broad multitude of many-body methods. Finally, an experimentally feasible tomography protocol has been recently proposed for dot-cavity devices, giving access to the relevant single-site and two-site RDM [59]. Hence we prospect cross-fertilization with the emerging field of entanglement certification in realistic open quantum impurity systems [60].

## IV. RESULTS

In this section we present numerical results for the evolution of quasilocal entanglement and correlations, as functions of the ratio $U/D$ across the interaction driven metal-insulator transition. The critical interaction for the transition depends on the size of the cluster $N_{\mathrm{imp}}$. We tracked the transition point for all the investigated cases and estimated it to be placed in the interval $U/D = [1.5, 1.6]$, although a precise determination of the transition point is beyond the scope of this work.

### A. Mott transition in the entanglement entropy

We begin by investigating the local and the nearest-neighbor entanglement entropies across the Mott transition. In Fig. 1 we report the behavior of $s_i$ and $s_{\langle ij \rangle}$ as a function of the interaction strength. We compare
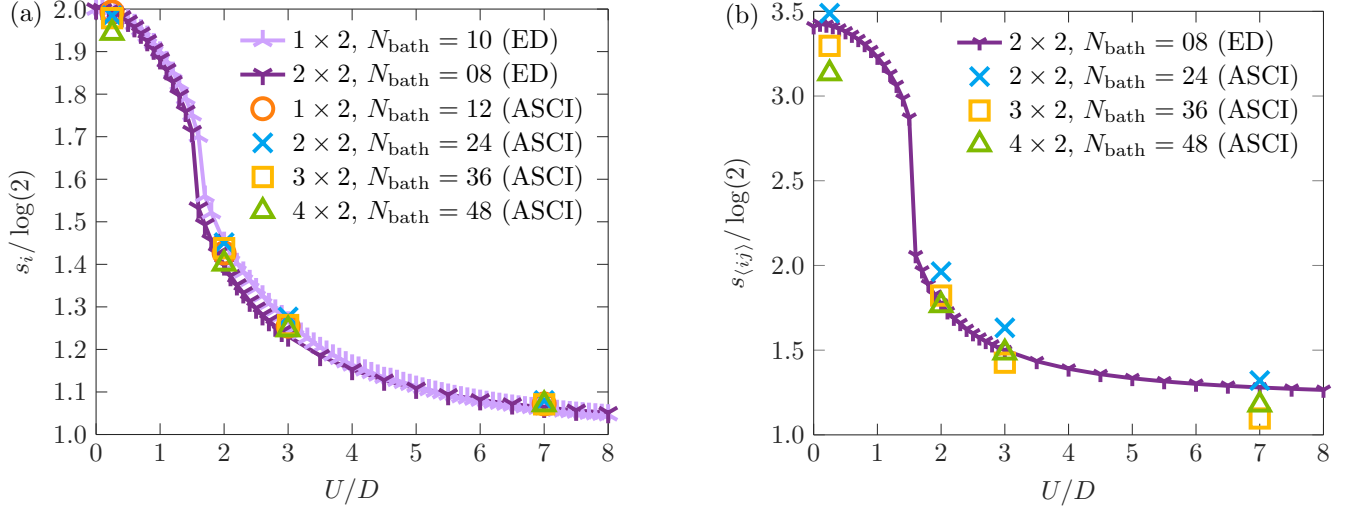
FIG. 1. Local (a) and nearest-neighbor (b) entanglement entropies, respectively $s_i$ and $s_{\langle ij \rangle}$, as a function of the interaction strength $U$ across the metal-insulator transition. Data from ED (lines and symbols) and ASCI (open symbols) and for different combinations of cluster sizes and bath levels. Clusters have the shape $N \times 2$.

the results for different cluster sizes and effective bath realizations, from both ED and ASCI methods.

The local entanglement entropy, see Fig. 1(a), is essentially insensitive to the cluster size, even in the proximity of the transition point at intermediate interaction values. This confirms that the entanglement between a single-site and its environment is properly captured in CDMFT and that this quantity, extensively treated in the recent literature [18–20], indeed represents a suitable marker for the Mott transition.

The nearest-neighbor entanglement entropy $s_{\langle ij \rangle}$, see Fig. 1(b), displays a more noticeable scaling with respect to the system size. In particular, major quantitative discrepancies arise between clusters of different sizes in the metallic and insulating regimes. We relate this behavior to the fact that some choices of the cluster shape (*e.g.* $3 \times 2$ and $4 \times 2$) can break the symmetries of the full lattice. However, according to their qualitative behavior across the Mott transition we can interpret the nearest-neighbor entanglement entropy to be well converged.

Having clarified the behavior of the local and nearest-neighbor entanglement entropies with respect to system size, in the following we shall focus on the $2 \times 2$ cluster for an in-depth analysis of the entanglement properties. A more thorough study of the scaling of the results beyond the nearest-neighbor limit in larger clusters will be investigated in Sec. IV C to further characterize the non-locality of classical and quantum correlations.

To start, we study the behavior of the entanglement entropies in the two limiting regimes of interaction. In the noninteracting limit $U \ll D$ the local entanglement entropy approaches the value $s_i = 2 \log(2)$, corresponding to a maximally entangled single-site state, for a half-filled noninteracting metal featuring equal populations of

empty, doubly and singly occupied electronic states. On the contrary we have not a maximally entangled state for nearest-neighbor sites, so the corresponding two-site entanglement entropy attains a value smaller than $4 \log(2)$. This is a direct consequence of the spatial correlation between the sites $i$ and $j$: if $s_{\langle ij \rangle} = 4 \log(2)$, then we would have $I_{\langle ij \rangle} = 0$, which according to Eq. 5 would imply that no finite correlator exist between the two neighboring sites. Nevertheless, a spectral analysis of the nearest-neighbor RDM reveals that, in this regime, all the 16 pure states contribute, although differently, to the configuration of the system, as expected for the noninteracting character of the solution.

In the strong coupling regime, $U \gg D$, both the local and nearest-neighbor von Neumann entropies appear to approach $\log(2)$. Yet, a deeper analysis of the underlying pure states reveals remarkable differences in the two corresponding density matrices. The local entanglement entropy is largely dominated by the equally weighted two pure states $|\uparrow\rangle$ and $|\downarrow\rangle$, namely the well-known local description of a paramagnetic Mott insulator. On the other hand, $s_{\langle ij \rangle}$ is dominated by four pure states, the spin-singlet $(|\uparrow\downarrow\rangle - |\downarrow\uparrow\rangle)/\sqrt{2}$, accounting for about 75% of the statistical mixture, and the spin-triplet states $|\uparrow\uparrow\rangle$, $|\downarrow\downarrow\rangle$ and $(|\uparrow\downarrow\rangle + |\downarrow\uparrow\rangle)/\sqrt{2}$, adding up for almost all the rest, in equal parts. Such relative composition of singlet and triplet states in the nearest-neighbor dimer has been checked to be consistent across all the addressed cluster and bath sizes: the numerical differences in the von Neumann entropies for the larger clusters are due to a different cumulative weight of all the remnant 12 pure states. This once again confirms that the two-site reduced density matrices are qualitatively consistent across all the cluster realizations.
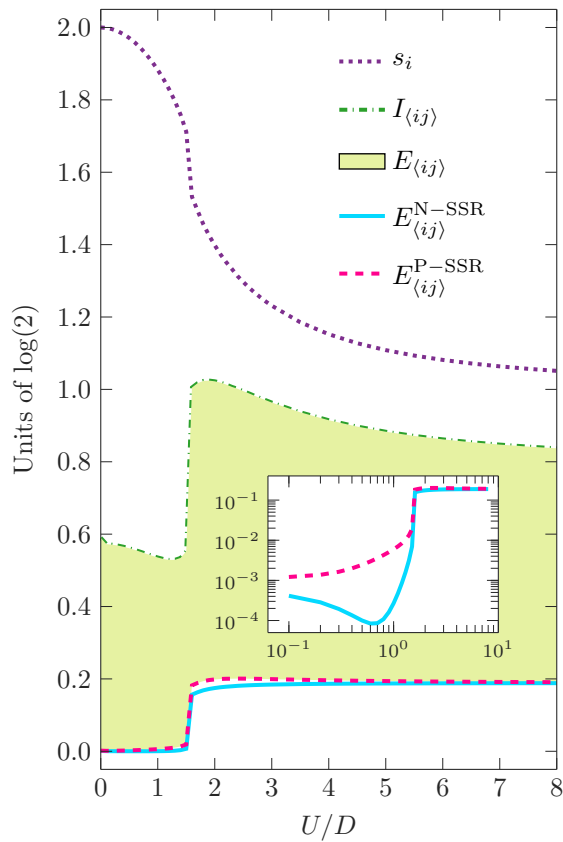
FIG. 2. Local entanglement entropy $s_i$, nearest-neighbor total correlation $I_{\langle ij \rangle}$ and the number (parity) superselected nearest-neighbor entanglement $E_{\langle ij \rangle}^{\text{N(P)-SSR}}$ as a function of the interaction strength. The latter curves are also reported in logarithmic scale in the inset, highlighting the different behavior in the Fermi liquid. The shaded area defines the range in which the unconstrained nearest-neighbor entanglement $E_{\langle ij \rangle}$ lies. Data from $2 \times 2$ cluster calculations using ED method with $N_{\text{bath}} = 8$.

## B. Entanglement between nearest neighbors

Here, we investigate in more detail the quantum correlation between adjacent lattice sites using the $2 \times 2$ plaquette CDMFT/ED solution of the model, which captures the essential features of the local and nearest-neighbor density matrices. In Fig. 2 we show the nearest-neighbor total correlation $I_{\langle ij \rangle}$ and the particle number (parity) superselected nearest-neighbor entanglement $E_{\langle ij \rangle}^{\text{N(P)-SSR}}$, compared to the well-known behavior of the local entanglement entropy $s_i$. Considering the bounds $E_{\langle ij \rangle}^{\text{N(P)-SSR}} \leq E_{\langle ij \rangle} \leq I_{\langle ij \rangle}$, we can identify a region (shaded area in Fig. 2) in which the unconstrained nearest-neighbor entanglement lies. Remarkably, both the upper and lower bounds to $E_{\langle ij \rangle}$ show a sudden rise at the Mott transition, in sharp contrast with the local entanglement entropy which is monotonically suppressed as the interaction is increased. This is a key result of this

work that we can rationalize as follows. The local entanglement entropy includes contributions for all spatial ranges [25]. Conversely, $E_{\langle ij \rangle}$ takes into account only the entanglement across a single lattice bond. Thus, when looking at the spatial entanglement of the system through $s_i$, the Mott insulator might appear less correlated than a Fermi liquid state. Instead, the nearest-neighbor entanglement undergoes an abrupt boost at the transition, recovering the usual picture of Mott insulators as locally strongly correlated phases of matter. We interpret this result as a signature of the intimate relationship between strong correlations and (Mott) localization.

We can push the resulting physical picture further by focusing on the comparison between the local entanglement entropy and the nearest-neighbor total correlation. Elaborating on the strong subadditivity property of the von Neumann entropies [61] we can write the following inequality (see Appendix B)

$$\bar{I}_{ij} \stackrel{\text{def}}{=} \frac{1}{\ell - 1} \sum_{j \neq i} I_{ij} \leq 2s_i, \tag{12}$$

where $\ell$ is the number of sites in the cluster and we recall that $I_{ij}$ represents the total correlation between two impurity sites $i$ and $j$. Hence the local entanglement entropy bounds from above the *cluster-averaged* two-site total correlation $\bar{I}_{ij}$. The expression for $\bar{I}_{ij}$ contains $\zeta$ identical terms, namely $I_{\langle ij \rangle}$, with $\zeta$ the number of nearest neighbors of site $i$ in the cluster. We can assume that the remaining terms in the expression for $\bar{I}_{ij}$ decay with the intersite distance [31, 62]. Their contribution is then at most a negative additive shift to the value of the local entanglement entropy. This explains the similar tail behavior of $s_i$ and $I_{\langle ij \rangle}$ in the Mott regime and implies that the total correlation in the Mott phase is more local, namely has shorter range, than the quantum entanglement of a Fermi liquid state. More evidence about the quasilocal nature of entanglement and correlations in Mott insulators will be given in Sec. IV C.

Finally, we note that both $E_{\langle ij \rangle}^{\text{P-SSR}}$ and $E_{\langle ij \rangle}^{\text{N-SSR}}$ essentially vanish throughout the whole metallic phase and quickly saturate to their maximum value in the Mott insulator. The presence of two sharply distinct entanglement scales clearly identifies the two phases, suggesting that these superselected measures are able to capture the adiabatic connection to either the noninteracting and the strong coupling limit, at all intermediate strongly correlated regimes. It is worth remarking that a deeper inspection (inset in Fig. 2) reveals a qualitatively different behavior of $E_{\langle ij \rangle}^{\text{P-SSR}}$ and $E_{\langle ij \rangle}^{\text{N-SSR}}$, throughout the Fermi liquid. After the Mott transition the superselection rules instead become quickly indistinguishable on the nearest-neighbor entanglement. This can be readily understood by looking at their expressions, see Eqs. A5 and A6: the two quantities differ by a term depending on the populations of doublons and holons, which asymptotically vanish in the Mott phase.
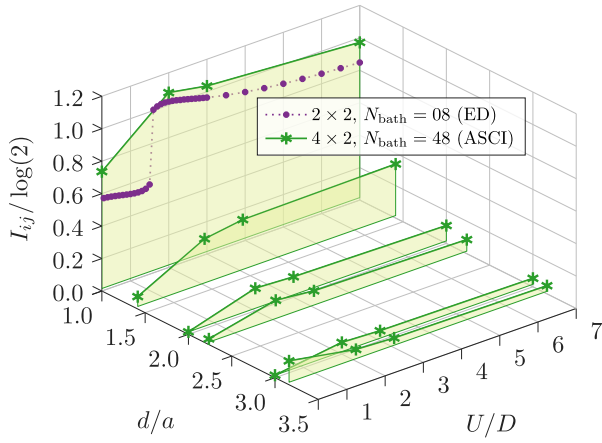
FIG. 3. Two-site total correlation $I_{ij}$ as a function of inter-site distance $d/a$ (with $a$ the lattice spacing) and interaction strength $U/D$. For $d/a = 1$ it reduces to the nearest-neighbor total correlation $I_{\langle ij \rangle}$ (see main text). Data from ASCI calculations using $4 \times 2$ cluster size (star symbols and solid lines) and ED calculations for $d/a = 1$ using $2 \times 2$ cluster (filled symbols and dotted line). The shaded area represents $E_{ij} \leq I_{ij}$, namely the range in which lies the nonlocal entanglement between the two selected sites.

## C. Entanglement beyond nearest neighbors

Having clarified the behavior of the two-site entanglement for the minimal lattice distance, we now devote our attention to its scaling beyond nearest neighbors. To this end we consider a $4 \times 2$ cluster which we address using the ASCI method for CDMFT. In Fig. 3 we show the total correlations $I_{ij}$ between two lattice sites $i$ and $j$, at increasing distances. In particular we choose the lower left corner site of the cluster as $i$, and vary $j$ as to select all the intracluster distances $d = a, \sqrt{2}a, 2a, \sqrt{5}a, 3a, \sqrt{10}a$, where $a$ is the lattice constant. Given that $I_{ij}$ represents an upper bound for the two-site entanglement, we can readily infer that the two-site quantum correlations are quickly damped with distance. Remarkably, the increase of two-site correlations at the Mott transition observed for nearest-neighbor pairs is progressively smoothed at larger distances. These findings further underline the quasilocal nature of the two-site entanglement across the whole phase diagram of the model, with the Mott insulator likely to have even a shorter range with respect to its parent Fermi liquid state.

## V. ROBUSTNESS WITH RESPECT TO SSR

We sharpen our analysis by applying the N-SSR and the P-SSR to the local entanglement entropy and the nearest-neighbor total correlation. This will enable us to understand how these quantities are affected by the superselection rules, which are expected to give the hallmark of experimentally accessible correlations in a realis-
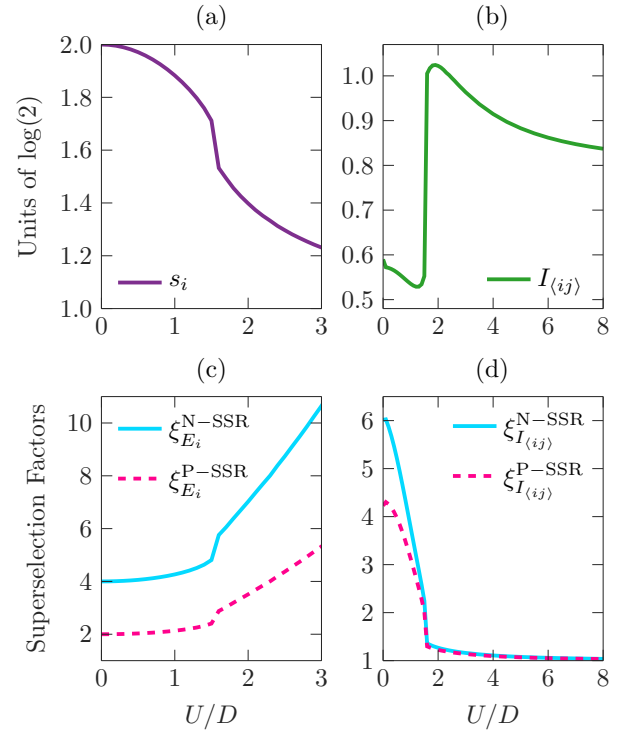


FIG. 4. Local entanglement entropy (a), nearest-neighbor total correlation (b) and their respective [(c) and (d)] particle number and parity superselection factors $\xi_{E_i}^{\mathrm{N(P)\text{-}SSR}}$ and $\xi_{I_{\langle ij \rangle}}^{\mathrm{N(P)\text{-}SSR}}$, as a function of the interaction strength. Data from ED calculations with a $2 \times 2$ cluster and $N_{\mathrm{bath}} = 8$ bath levels.

tic setup based on operations performed onto individual local electronic degrees of freedom [32, 33, 36–44].

In Fig. 4, we report the local entanglement entropy $s_i$ and the nearest-neighbor total correlation $I_{\langle ij \rangle}$ together with the respective superselection factors, as defined in Eqs. 9, 10. The explicit expressions of these two quantities can be retrieved from Appendix A, see Eqs. A1, A2 and Eqs. A3, A4 respectively. These factors quantify the weight that the superselection rules filter out from the corresponding correlation measures.

In the Fermi liquid both factors are strongly enhanced by the SSR, signaling that correlations and entanglement in a metal are not really accessible via standard local operations. This matches with the results previously discussed in Fig. 2: the most localized bipartite entanglement measure we can define on a lattice vanishes in an interacting metal, provided that we preclude any local fluctuation of charge. The local entanglement and two-site correlations, measured by $s_i$ and $I_{\langle ij \rangle}$, are then ascribed to the itinerant nature of the electronic state.

Remarkably, in the correlation-driven insulator we observe a dramatic differentiation between the two markers. The single-site entanglement entropy superselection factors $\xi_{E_i}^{\mathrm{N(P)\text{-}SSR}}$ linearly increase with the on-site repulsion. On the contrary, $\xi_{I_{\langle ij \rangle}}^{\mathrm{N(P)\text{-}SSR}}$ steadily approach the

unity right after the transition point, signalling that the results are increasingly robust with respect to the SSR, *i.e.* the filtering is nearly irrelevant in this regime.

The fact that $s_i$ is damped by superselection rules while the nearest neighbor total correlation becomes essentially insensitive to them, as we enter the Mott phase, suggests that nearest-neighbor quantities are better suited for the characterization of correlated insulators. Indeed, the signature of Mott physics is the freezing of local charge fluctuations thus the N-SSR would constitute a natural physical stage to reveal the underpinning role of strong correlations.

The robustness of the nearest-neighbor total correlation to N-SSR and P-SSR and the fact that $E_{\langle ij \rangle}^{\mathrm{N\text{-}SSR}} \simeq E_{\langle ij \rangle}^{\mathrm{P\text{-}SSR}}$ deep in the Mott insulating phase, suggests that the nearest-neighbor entanglement $E_{\langle ij \rangle} \leq I_{\langle ij \rangle}$ could share the same property with respect to the SSR. In this case, we expect the full unrestricted quantity to be significantly close to its lower bound shown in Fig. 2.

## VI. CONCLUSIONS AND OUTLOOK

The local entanglement entropy has been extensively studied through the last decade to revisit the physics of the Mott transition under the lens of quantum information theory [17–20]. Although this quantity allows for a full characterization of the quantum phase transition and both its sub- and super-critical thermal signatures, its physical interpretation has been hindered by the lack of a clear distinction between genuinely local and nonlocal contributions [25].

Based on a CDMFT analysis of the two dimensional Hubbard model we clarified the role of local and *quasilocal* entanglement across the Mott transition. In particular, we leveraged a notion of entanglement between a pair of sites, with no reference to their environment. This quantity gives a genuine measure of the quasilocal entanglement in the ground state. Despite being well defined as the relative entropy of entanglement, such two-site entanglement has no accessible general expression and its determination represents an open problem in quantum information theory [35]. Consequently, we carefully analyze upper and lower bounds to the two-site entanglement. The former is obtained by a rigorous interpretation of the mutual information as a measure of maximal total correlations, while the latter are based on recently introduced expression for the two-site entanglement under charge and parity superselection rules [32], amounting to constrain the possible coherent superposition of quantum states to those conserving the local electron number or its parity.

We proved that the nearest-neighbor total correlation is almost unaffected by the local charge and parity superselection rules, in the Mott insulator. On the other hand the charge and parity superselected two-site entanglement formulas have been proven indistinguishable in the Mott phase. Hence we propose the two-site measures

of entanglement and correlation as reliable tools for the study of (Mott) localized phases of matter.

Following the evolution of the entanglement bounds as a function of the interaction strength, we predict a sharp increase of the nearest-neighbor entanglement at the Mott transition point, in contrast with the well-known phenomenology of the local entanglement entropy. Consequently, while the Mott insulator might globally result less spatially entangled than the weak coupling Fermi liquid state, we argue that the genuine quasilocal quantum correlation is actually increased by Mott localization, thus reconciling with the paradigmatic view of a Mott insulator as a strongly correlated localized system. Further evidence about the quasilocal nature of the two-site entanglement, in both the Fermi liquid and Mott regimes, has been secured by extending our analysis beyond nearest neighbors.

Our results shed new light on the mechanism underlying the transformation of a Fermi liquid metal into a strongly correlated insulator, namely the Mott transition, bridging the fertile field of quantum information theory with the notoriously tough problem of describing strongly correlated electrons. The analysis is based on CDMFT calculations with clusters sizes up to eight sites, providing a reasonably complete description of the Mott transition, as extensively studied and compared with other methods, including larger clusters [63, 64]. The addressed cluster sizes allow us for a systematic and computationally affordable study in a well-documented setting. There are several directions to verify the robustness of our results, including the analysis of larger clusters within CDMFT or dynamical cluster approximations [22], or even the adoption of different algorithms ranging from quantum Monte Carlo to tensor networks [65–67]. However, we emphasize that our results provide a clear characterization of the entanglement properties of the metallic and insulating solutions, which is expected to be valid regardless of the approximation we used to identify it.

Different fruitful research directions can be envisaged in this respect. Our information theory perspective can indeed provide precious information on the intriguing analogy between nonlocal correlations of the single-band Hubbard model and correlations between different local orbitals in multi-orbital systems [68–70] and, in more general terms, identify a conceptual framework to address the role of nonlocal correlations arising from local interactions in multi-component quantum systems including unconventional superconductors [71], correlated topological insulators [72, 73] and SU(N) cold-atom systems [74, 75].

## Appendix A: Explicit formulas for superselected local entanglement, two-site total correlation and two-site entanglement

In the following we will report the explicit expressions for the charge and parity *superselected* measures of correlation and entanglement, as discussed in the main body of the paper. Particularly we will address

- the superselected entanglement between a single-site and its environment (Eqs. A1 and A2),

- the superselected total correlation between two neighboring sites (Eqs. A3 and A4)

- the superselected entanglement between two neighboring sites (Eqs. A5 and A6)

While fixing notations and language, we will also briefly comment on the physical meaning of these superselection rules and warn the reader about easy pitfalls on the interpretation of the results, so to make our results as precise as we can. Proofs will not be addressed but we will give explicit pointers to the relevant literature.

Given the spin SU(2) and charge U(1) symmetries of the Hubbard model, the reduced density matrix for a single site $\rho_i$ is diagonal in the basis $|\bullet\rangle$, $|\uparrow\rangle$, $|\downarrow\rangle$, $|\uparrow\downarrow\rangle$, where the black dot represents an empty site.

$$\rho_i = \begin{pmatrix} p_1 & 0 & 0 & 0 \\ 0 & p_2 & 0 & 0 \\ 0 & 0 & p_3 & 0 \\ 0 & 0 & 0 & p_4 \end{pmatrix}$$

If no superselection rule is taken into account and the ground state of the full lattice is *pure*, we can write it as Schmidt decomposition

$$
\begin{aligned}
|\Psi_{\mathrm{gs}}\rangle = {} & \sqrt{p_1}\,|\bullet\rangle \;\otimes\; |N, M\rangle + \\
& \sqrt{p_2}\,|\uparrow\rangle \;\otimes\; |N-1, M-\tfrac{1}{2}\rangle + \\
& \sqrt{p_3}\,|\downarrow\rangle \;\otimes\; |N-1, M+\tfrac{1}{2}\rangle + \\
& \sqrt{p_4}\,|\uparrow\downarrow\rangle \otimes\; |N-2, M\rangle,
\end{aligned}
$$

where $|\mathcal{N}, \mathcal{M}\rangle$ represent a Fock state of $\mathcal{N}$ electrons and $\mathcal{M}$ magnetization, living on all lattice sites $j \neq i$.

In this case, the entanglement between the single site $i$ and the rest of the lattice $\{j \neq i\}$, which we shall refer to as $E_i$, is just given by the von Neumann entropy of $\rho_i$, namely

$$E_i \equiv s_i = -\sum_n p_n \log p_n.$$

However, as soon as we consider a superselection rule, namely a local restriction on the allowed physical operators, such that all of them must commute with a given conserved quantity $\mathcal{Q}_i$, the ground state $\Psi_{\mathrm{gs}}$ must be projected into the eigensubspaces of $\mathcal{Q}_i$, defining the block diagonal *superselected* density matrix

$$\rho_{\mathrm{gs}}^{\mathcal{Q}\text{-SSR}} = \sum_i \left| \Psi_{\mathrm{gs}}^{\mathcal{Q}_i} \right\rangle\!\!\left\langle \Psi_{\mathrm{gs}}^{\mathcal{Q}_i} \right|.$$

In general, the purity of $\rho_{\mathrm{gs}}^{\mathcal{Q}\text{-SSR}}$ cannot be guaranteed, so that all its von Neumann reduced entropies (including the single-site entropy) are not legitimate measures of entanglement

$$E_i^{\mathcal{Q}\text{-SSR}} \neq -\sum_n p_n^{\mathcal{Q}\text{-SSR}} \log p_n^{\mathcal{Q}\text{-SSR}}.$$

A careful treatment, based on a general definition of entanglement as the minimal distance (quantum relative entropy) of the given superselected local density matrix from the set of separable single-site states [34], leads instead to the following expressions

$$
\begin{aligned}
E_i^{\mathrm{N\text{-}SSR}} = {} & (p_2 + p_3) \log(p_2 + p_3) \qquad \text{(A1)} \\
& - p_2 \log p_2 - p_3 \log p_3
\end{aligned}
$$

$$
\begin{aligned}
E_i^{\mathrm{P\text{-}SSR}} = {} & (p_1 + p_4) \log(p_1 + p_4) \qquad \text{(A2)} \\
& + (p_2 + p_3) \log(p_2 + p_3) \\
& - p_1 \log p_1 - p_2 \log p_2 \\
& - p_3 \log p_3 - p_4 \log p_4
\end{aligned}
$$

for the cases of $\mathcal{Q}_i = N_i$ and $\mathcal{Q}_i = P_i$, being $N_i$ the local electron number and $P_i$ its parity. Notice that the $p_n$ entering the two expressions are the original elements of the $\rho_i$ local density matrix, since it is already diagonal on the $N_i$ and $P_i$ sectors. The full derivation can be found in Ref. [47].

Let us move on a two-site subsystem, described by the $\rho_{ij}$ reduced density matrix. Fixing a basis for the two-site Fock space as in Table I, we can define its matrix elements as $p_{nm} = \langle \psi_n | \rho_{ij} | \psi_m \rangle$. Again, the spin SU(2) and charge U(1) symmetries of the Hubbard model impose several restrictions on which $p_{nm}$ elements vanish, basically disallowing all fluctuations in the two-site charge and magnetization. Applying the number superselection rule (N-SSR) amounts to forbidding all changes in the
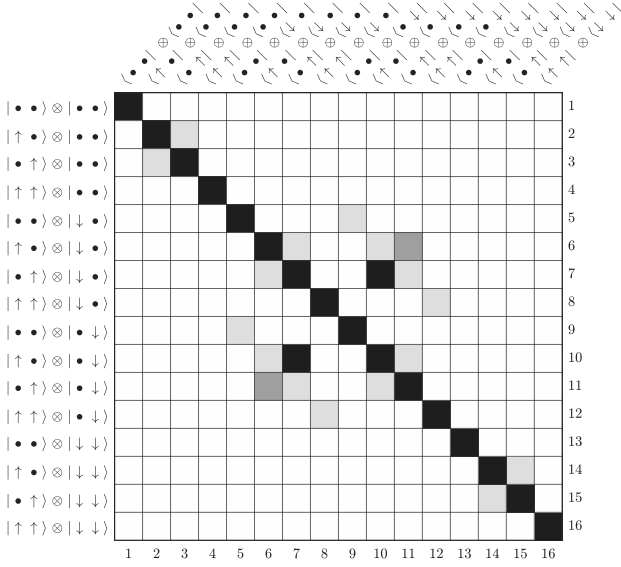
FIG. 5. Pictorial representation of the two-site reduced density matrix $\rho_{ij}$. For a generic interaction value $U/D$, most entries vanish (white) due to the spin and charge symmetries of the Hubbard model. Superselecting for local electron parity (P-SSR) sets all light-shaded entries to zero, while the N-SSR removes the remaining local charge fluctuations (the two dark-shaded entries). Black elements are always preserved.

| Label: $n$ | State: $\vert\psi_n^\uparrow\rangle \otimes \vert\psi_n^\downarrow\rangle$ |
|---|---|
| 1 | $\vert\bullet\,\bullet\rangle \otimes \vert\bullet\,\bullet\rangle$ |
| 2 | $\vert\uparrow\,\bullet\rangle \otimes \vert\bullet\,\bullet\rangle$ |
| 3 | $\vert\bullet\,\uparrow\rangle \otimes \vert\bullet\,\bullet\rangle$ |
| 4 | $\vert\uparrow\,\uparrow\rangle \otimes \vert\bullet\,\bullet\rangle$ |
| 5 | $\vert\bullet\,\bullet\rangle \otimes \vert\downarrow\,\bullet\rangle$ |
| 6 | $\vert\uparrow\,\bullet\rangle \otimes \vert\downarrow\,\bullet\rangle$ |
| 7 | $\vert\bullet\,\uparrow\rangle \otimes \vert\downarrow\,\bullet\rangle$ |
| 8 | $\vert\uparrow\,\uparrow\rangle \otimes \vert\downarrow\,\bullet\rangle$ |
| 9 | $\vert\bullet\,\bullet\rangle \otimes \vert\bullet\,\downarrow\rangle$ |
| 10 | $\vert\uparrow\,\bullet\rangle \otimes \vert\bullet\,\downarrow\rangle$ |
| 11 | $\vert\bullet\,\uparrow\rangle \otimes \vert\bullet\,\downarrow\rangle$ |
| 12 | $\vert\uparrow\,\uparrow\rangle \otimes \vert\bullet\,\downarrow\rangle$ |
| 13 | $\vert\bullet\,\bullet\rangle \otimes \vert\downarrow\,\downarrow\rangle$ |
| 14 | $\vert\uparrow\,\bullet\rangle \otimes \vert\downarrow\,\downarrow\rangle$ |
| 15 | $\vert\bullet\,\uparrow\rangle \otimes \vert\downarrow\,\downarrow\rangle$ |
| 16 | $\vert\uparrow\,\uparrow\rangle \otimes \vert\downarrow\,\downarrow\rangle$ |

TABLE I. Basis for the two-site Fock space $\mathcal{F}_{ij}$. The indices $n$ of the quantum states $\vert\psi_n\rangle = \vert\psi_n^\uparrow\rangle \otimes \vert\psi_n^\downarrow\rangle$ define the conventional labeling for the matrix elements $p_{nm}$ of the reduced density matrix for the two-site subsystem. Black dots ($\bullet$) represent empty lattice sites.

local (single-site) charge, while the parity superselection rule (P-SSR) allows only the charge fluctuations that preserve the parity of the local particle number. Local spin-flips survive both superselection rules, as they commute with the local particle number. A schematic depiction of the structure of $\rho_{ij}$, and how it changes under N-SSR and P-SSR is reported in Fig. 5. Once either the N-SSR or the P-SSR filtering is applied on $\rho_{ij}$, the superselected nearest-neighbor total correlation is just given by the mutual information between its reduced single-site subsystems. In functional terms, if we refer to the von Neumann entropy of a generic density matrix $\rho$ as $s\{\rho\}$, we have

$$I_{ij}^{\text{N-SSR}} = s\{\rho_i\} + s\{\rho_j\} - s\left\{\rho_{ij}^{\text{N-SSR}}\right\}, \qquad \text{(A3)}$$

$$I_{ij}^{\text{P-SSR}} = s\{\rho_i\} + s\{\rho_j\} - s\left\{\rho_{ij}^{\text{P-SSR}}\right\}. \qquad \text{(A4)}$$

We stress that the single-site reduced density matrices $\rho_i$, as computed from $\rho_{ij}$ via the usual partial trace, are insensitive to the N-SSR and P-SSR filtering, hence not superscripted in the formulas. Once again, note that while the superselected total correlation is still mathematically given by a subtraction of von Neumann entropies, the latter are not anymore legitimate measures of the entanglement between single- / pairs of sites and their surroundings. Hence the superselected total correlation cannot be physically interpreted as an algebraic sum of superselected entanglement measures. An extended discussion on all these subtle aspects can be found in Ref. [12].

As discussed in the main body of the paper, we target the entanglement between a pair of local orbitals, defined as a suitable minimal "distance" (namely the quantum relative entropy) between the given reduced density matrix $\rho_{ij}$ and the set of separable two-site states $\mathcal{D}_{ij}$ [34]. The relevant minimization process constitutes a formidable open problem in quantum information theory, given that no efficient description for the boundary of the $\mathcal{D}_{ij}$ set is known [35]. Recently a set of closed formulas has been proposed, under the assumption of either N-SSR or P-SSR, plus some typical symmetries of condensed matter systems [32]. In particular, we adopt here the versions valid under conservation of global $N$ and $S^z$, particle-hole symmetry and the assumption of a singlet ground state for the whole lattice, as they are indeed all satisfied by both the Hubbard model on the half-filled $2d$ square lattice and its CDMFT solution.
Here we report these two closed expressions, commenting on their physical properties with respect to the numerical results presented in Fig. 2. The reader interested in derivations and a general discussion on the relevance for arbitrary condensed matter systems and realistic quantum information processing therein, is strongly encouraged to approach the original references [32, 33].

With reference to Table I, we define the following probabilities

$$p_n = \langle \psi_n | \rho_{ij} | \psi_n \rangle, \quad \forall \, n \in [1, 16] \setminus \{6, 7, 10, 11\},$$

$$\begin{pmatrix} p_6 \\ p_{11} \end{pmatrix} = R^\dagger \begin{pmatrix} \langle \psi_6 | \rho_{ij} | \psi_6 \rangle & \langle \psi_6 | \rho_{ij} | \psi_{11} \rangle \\ \langle \psi_{11} | \rho_{ij} | \psi_6 \rangle & \langle \psi_{11} | \rho_{ij} | \psi_{11} \rangle \end{pmatrix} R,$$

$$\begin{pmatrix} p_7 \\ p_{10} \end{pmatrix} = R^\dagger \begin{pmatrix} \langle \psi_7 | \rho_{ij} | \psi_7 \rangle & \langle \psi_7 | \rho_{ij} | \psi_{10} \rangle \\ \langle \psi_{10} | \rho_{ij} | \psi_7 \rangle & \langle \psi_{10} | \rho_{ij} | \psi_{10} \rangle \end{pmatrix} R,$$

$$\text{with } R = \begin{pmatrix} 1 & -1 \\ 1 & +1 \end{pmatrix} \times \frac{1}{\sqrt{2}}.$$

Note that, according to symmetries, $\langle \psi_7 | \rho_{ij} | \psi_7 \rangle = \langle \psi_{10} | \rho_{ij} | \psi_{10} \rangle$ and $\langle \psi_6 | \rho_{ij} | \psi_6 \rangle = \langle \psi_{11} | \rho_{ij} | \psi_{11} \rangle$, so that the rotation matrix $R$ has been defined here as to diagonalize the subspaces defined by Span$\{|\psi_7\rangle, |\psi_{10}\rangle\}$ and Span$\{|\psi_6\rangle, |\psi_{11}\rangle\}$, namely the only nondiagonal blocks surviving the superselection filtering on $\rho_{ij}$ (see Fig. 5). It can be further proven that the only relevant probabilities for determining the N-SSR and P-SSR two-site entanglement measures are $p_1 = p_{16}$ (equality ensured by particle-hole symmetry), $p_4 = p_{13}$ (equality ensured by a singlet ground state), $p_6, p_{11}, p_7$ and $p_{10}$.

Finally we can express the charge and parity superselected two-site entanglement measures as

$$E_{ij}^{\text{N-SSR}} = \left[ r \log \left( \frac{2r}{r+t} \right) + t \log \left( \frac{2t}{r+t} \right) \right] \times \theta(t-r), \tag{A5}$$

$$E_{ij}^{\text{P-SSR}} = E_{ij}^{\text{N-SSR}} + \left[ s \log \left( \frac{2s}{s+\tau} \right) + \tau \log \left( \frac{2\tau}{s+\tau} \right) \right] \times \theta(\tau-s), \tag{A6}$$

where $\theta(t-r)$ and $\theta(\tau-s)$ are Heaviside steps, vanishing if $r \geq t$, and $s \geq \tau$, respectively, where

$$t = \max\{p_7, p_{10}\}, \quad r = \min\{p_7, p_{10}\} + p_4 + p_{13},$$
$$\tau = \max\{p_6, p_{11}\}, \quad s = \min\{p_6, p_{11}\} + p_1 + p_{16}.$$

The vanishing imposed by the $\theta$-steps reflects the Peres–Horodecki separability criterion [76–78].

We highlight that Eqs. A5 and A6 differ for a term depending on $\tau$ and $s$ alone, which involve only diagonal occupations of pairs of *doublon* and *holon* states. Since both of them are gradually suppressed by Mott localization we expect the two superselected measures of two-site entanglement to be asymptotically indistinguishable in the Mott insulator.

## Appendix B: Deriving a sum-rule for the two-site mutual information from the strong superadditivity property of quantum von Neumann entropies

For any state of a generic quantum tripartite system $\mathcal{H}_{\text{ABC}} = \mathcal{H}_{\text{A}} \otimes \mathcal{H}_{\text{B}} \otimes \mathcal{H}_{\text{C}}$, a *strong subadditivity* property has been proven to relate the von Neumann entropies of all its subsystems and the whole density matrix $\rho_{\text{ABC}}$. In standard notation it reads [61]

$$s(\rho_{\text{ABC}}) + s(\rho_{\text{B}}) \leq s(\rho_{\text{AB}}) + s(\rho_{\text{BC}}). \tag{B1}$$

Adding the von Neumann entropy of subsystem A on both sides, we can recast the inequality in terms of suitable mutual informations, as

$$s(\rho_{\text{ABC}}) + s(\rho_{\text{A}}) + s(\rho_{\text{B}}) \leq s(\rho_{\text{AB}}) + s(\rho_{\text{A}}) + s(\rho_{\text{BC}})$$

$$s(\rho_{\text{A}}) + s(\rho_{\text{B}}) - s(\rho_{\text{AB}}) \leq s(\rho_{\text{A}}) + s(\rho_{\text{BC}}) - s(\rho_{\text{ABC}})$$

$$I(\rho_{\text{A}} : \rho_{\text{B}}) \leq I(\rho_{\text{A}} : \rho_{\text{BC}}) \tag{B2}$$

Let us consider the CDMFT solution for the Hubbard model and take A and B as single-site orbitals $i, j$ in the cluster and C as the rest of the impurity model. Equation B2 then becomes $I_{ij} \leq I_{i\{k \neq i\}}$. Since the ground state of the impurity model is pure, we have $I_{i\{k \neq i\}} = s_i + s_{\{k \neq i\}} = 2s_i$ and we can further recast the inequality as

$$I_{ij} \leq 2s_i, \quad \forall \, i \neq j \tag{B3}$$

Finally we fix a reference site $i$ and sum over all other possible cluster sites $j \neq i$, to get

$$\sum_{j=1}^{N_{\text{imp}}} I_{ij}(1 - \delta_{ij}) \leq \sum_{j=1}^{N_{\text{imp}}} 2s_i(1 - \delta_{ij})$$

$$\frac{\sum_{j=1}^{N_{\text{imp}}} I_{ij}(1 - \delta_{ij})}{2 \sum_{j=1}^{N_{\text{imp}}} (1 - \delta_{ij})} \leq s_i \tag{B4}$$

which is equivalent to Eq. 12 in the main text.

## Appendix C: Comparative table of entanglement markers for strongly correlated electrons

For ease of reference, here we provide a concise summary of all the correlation and entanglement markers we discuss throughout this work. We assume zero temperature and a general mixed state for the single- and two-site subsystems, due to the embedding in the lattice.

| MARKER | | WHAT IT MEASURES | WHAT IT BOUNDS |
|---|---|---|---|
| Single-site entanglement entropy (2) | $s_i$ | Entanglement between a single site $i$ and the rest of the lattice, for pure ground states | — |
| Single-site entanglement under charge SSR (A1) | $E_i^{\text{N-SSR}}$ | Accessible entanglement between a single site $i$ and the rest of the lattice, within operations that conserve the local charge $N_i$ | Entanglement between a single site $i$ and the rest of the lattice, for all ground states [from below] |
| Single-site entanglement under parity SSR (A2) | $E_i^{\text{P-SSR}}$ | Accessible entanglement between a single site $i$ and the rest of the lattice, within operations that conserve the parity of the local electron number $N_i$ | Entanglement between a single site $i$ and the rest of the lattice, for all ground states [from below] |
| Two-site entanglement entropy (3) | $s_{ij}$ | Entanglement between the two sites $(i,j)$ and the rest of the lattice, for pure ground states | — |
| Two-site mutual information (4) | $I_{ij}$ | Total correlation between the two sites $i$ and $j$ | The entanglement between $i$ and $j$, as well as any two-site correlator [from above] |
| Two-site mutual information under charge SSR (A3) | $I_{ij}^{\text{N-SSR}}$ | Accessible correlation between the two sites $i$ and $j$, within operations that conserve the local charge $N_i$ | The two-site mutual information $I_{ij}$ [from below] |
| Two-site mutual information under parity SSR (A4) | $I_{ij}^{\text{P-SSR}}$ | Accessible correlation between the two sites $i$ and $j$, within operations that conserve the parity of the local electron number $N_i$ | The two-site mutual information $I_{ij}$ [from below] |
| Two-site entanglement under charge SSR (A5) | $E_{ij}^{\text{N-SSR}}$ | Accessible entanglement between $i$ and $j$, within operations that conserve the local charge $N_i$ | The entanglement between $i$ and $j$. [from below] |
| Two-site entanglement under parity SSR (A6) | $E_{ij}^{\text{P-SSR}}$ | Accessible entanglement between $i$ and $j$, within operations that conserve the parity of the local electron number $N_i$ | The entanglement between $i$ and $j$. [from below] |

## Appendix D: Details of ASCI simulations

Here we provide some computational details of the ASCI calculations performed in this work for the different impurity models. As a reminder, a cluster with $N \times M$ correlated sites always has $6 \times N \times M$ bath sites.

As discussed in Refs. [30, 54, 55], the important parameters for the ASCI solver include: (i) the size of the Hilbert space truncation, (ii) the size of the core space, namely the subset of determinants from which the Hilbert space exploration at each iteration is started, (iii) the active space threshold value, and (iv) the excitation threshold for the Green's function calculation, namely from which ground state determinants to build excited states in order to complete the determinant truncation to improve the Green's function accuracy.

The $1\times2$ cluster impurity model calculations were done without any Hilbert space truncation, while the $2 \times 2$ calculations were done with a Hilbert space truncation of $10^5$ determinants. For the larger impurity models,

namely $3 \times 2$ and $4 \times 2$, the simulations with $U/D > 0.25$ were also performed with $10^5$ determinants, while the $U/D = 0.25$ simulation was performed with $5 \times 10^5$ determinants to ensure convergence of Green's function and von Neumann entropies with respect to the truncation size. In all cases, the core space from which to start the determinant search at each ASCI iteration (cf. Ref. [30]) was set equal to the full truncation. The threshold to define the active space in the approximate natural bath orbital basis was chosen to be $\delta = 10^{-4}$. Once the ASCI ground state energy is converged, we evaluate the Green's function after complementing the determinant truncation as described in Ref. [30, 57], namely adding determinants corresponding to single electron excitations (within and beyond the active space) on top of those determinants in the ASCI truncation with absolute wave function coefficients larger than $10^{-4}$. The DMFT self-consistency was iterated until the bath parameters were converged to an absolute error within $10^{-3}$, involving typically between 10 and 40 iterations.

[1] N. F. Mott, Metal-insulator transition, Rev. Mod. Phys. **40**, 677 (1968).

[2] M. Imada, A. Fujimori, and Y. Tokura, Metal-insulator transitions, Rev. Mod. Phys. **70**, 1039 (1998).

[3] A. Osterloh, L. Amico, G. Falci, and R. Fazio, Scaling of entanglement close to a quantum phase transition, Nature **416**, 608 (2002).

[4] T. J. Osborne and M. A. Nielsen, Entanglement in a simple quantum phase transition, Phys. Rev. A **66**, 032110 (2002).

[5] G. Vidal, J. I. Latorre, E. Rico, and A. Kitaev, Entanglement in quantum critical phenomena, Phys. Rev. Lett. **90**, 227902 (2003).

[6] L. Squillante, L. S. Ricco, A. M. Ukpong, R. E. Lagos-Monaco, A. C. Seridonio, and M. de Souza, Grüneisen parameter as an entanglement compass and the breakdown of the hellmann-feynman theorem, Phys. Rev. B **108**, L140403 (2023).

[7] A. Kitaev and J. Preskill, Topological entanglement entropy, Phys. Rev. Lett. **96**, 110404 (2006).

[8] M. Levin and X.-G. Wen, Detecting topological order in a ground state wave function, Phys. Rev. Lett. **96**, 110405 (2006).

[9] X. Chen, Z.-C. Gu, and X.-G. Wen, Local unitary transformation, long-range quantum entanglement, wave function renormalization, and topological order, Phys. Rev. B **82**, 155138 (2010).

[10] K. Boguslawski, P. Tecmer, G. Barcza, O. Legeza, and M. Reiher, Orbital entanglement in bond-formation processes, Journal of Chemical Theory and Computation **9**, 2959 (2013), pMID: 26583979.

[11] S. Szalay, G. Barcza, T. Szilvasi, L. Veis, and O. Legeza, The correlation theory of the chemical bond, Scientific Reports **7**, 2237 (2017).

[12] L. Ding, S. Knecht, Z. Zimborás, and C. Schilling, Quantum correlations in molecules: from quantum resourcing to chemical bonding, Quantum Science and Technology **8**, 015015 (2022).

[13] S. R. White, Density matrix formulation for quantum renormalization groups, Phys. Rev. Lett. **69**, 2863 (1992).

[14] O. Legeza and J. Sólyom, Optimizing the density-matrix renormalization group method using quantum information entropy, Phys. Rev. B **68**, 195116 (2003).

[15] C. J. Stein and M. Reiher, Automated selection of active orbital spaces, Journal of Chemical Theory and Computation **12**, 1760 (2016).

[16] A. Georges, G. Kotliar, W. Krauth, and M. J. Rozenberg, Dynamical mean-field theory of strongly correlated fermion systems and the limit of infinite dimensions, Rev. Mod. Phys. **68**, 13 (1996).

[17] D. D. Su, X. Dai, and N. H. Tong, Local entanglement entropy at the Mott metal-insulator transition in infinite dimensions, Modern Physics Letters B **27**, 1350034 (2013).

[18] C. Walsh, P. Sémon, D. Poulin, G. Sordi, and A.-M. S. Tremblay, Local entanglement entropy and mutual information across the Mott transition in the two-dimensional Hubbard model, Phys. Rev. Lett. **122**, 067203 (2019).

[19] C. Walsh, P. Sémon, D. Poulin, G. Sordi, and A.-M. S. Tremblay, Entanglement and classical correlations at the doping-driven Mott transition in the two-dimensional Hubbard model, PRX Quantum **1**, 020310 (2020).

[20] C. Walsh, M. Charlebois, P. Sémon, G. Sordi, and A.-M. S. Tremblay, Information-theoretic measures of superconductivity in a two-dimensional doped Mott insulator, Proceedings of the National Academy of Sciences **118**, e2104114118 (2021).

[21] G. Kotliar, S. Y. Savrasov, G. Pálsson, and G. Biroli, Cellular dynamical mean field approach to strongly correlated systems, Phys. Rev. Lett. **87**, 186401 (2001).

[22] T. Maier, M. Jarrell, T. Pruschke, and M. H. Hettler, Quantum cluster theories, Rev. Mod. Phys. **77**, 1027 (2005).

[23] H. Park, K. Haule, and G. Kotliar, Cluster dynamical

mean field theory of the Mott transition, Phys. Rev. Lett. **101**, 186403 (2008).

[24] E. Cocchi, L. A. Miller, J. H. Drewes, C. F. Chan, D. Pertot, F. Brennecke, and M. Köhl, Measuring entropy and short-range correlations in the two-dimensional Hubbard model, Phys. Rev. X **7**, 031025 (2017).

[25] L. Amico, R. Fazio, A. Osterloh, and V. Vedral, Entanglement in many-body systems, Rev. Mod. Phys. **80**, 517 (2008).

[26] S. Bera, A. Haldar, and S. Banerjee, Dynamical mean-field theory for Rényi entanglement entropy and mutual information in the hubbard model, Phys. Rev. B **109**, 035156 (2024).

[27] J. D'Emidio, R. Orús, N. Laflorencie, and F. de Juan, Universal features of entanglement entropy in the honeycomb hubbard model, Phys. Rev. Lett. **132**, 076502 (2024).

[28] M. Capone, L. de' Medici, and A. Georges, Solving the dynamical mean-field theory at very low temperatures using the Lanczos exact diagonalization, Phys. Rev. B **76**, 245116 (2007).

[29] A. Amaricci, L. Crippa, A. Scazzola, F. Petocchi, G. Mazza, L. de Medici, and M. Capone, EDIpack: A parallel exact diagonalization package for quantum impurity problems, Computer Physics Communications **273**, 108261 (2022).

[30] C. Mejuto-Zaera, N. M. Tubman, and K. B. Whaley, Dynamical mean field theory simulations with the adaptive sampling configuration interaction method, Phys. Rev. B **100**, 125165 (2019).

[31] M. M. Wolf, F. Verstraete, M. B. Hastings, and J. I. Cirac, Area laws in quantum systems: Mutual information and correlations, Phys. Rev. Lett. **100**, 070502 (2008).

[32] L. Ding, Z. Zimboras, and C. Schilling, Quantifying electron entanglement faithfully (2022), arXiv:2207.03377 [quant-ph].

[33] L. Ding, G. Dünnweber, and C. Schilling, Physical entanglement between localized orbitals, Quantum Science and Technology **9**, 015005 (2023).

[34] V. Vedral, The role of relative entropy in quantum information theory, Rev. Mod. Phys. **74**, 197 (2002).

[35] O. Krueger and R. F. Werner, Some open problems in quantum information theory (2005), arXiv:quant-ph/0504166 [quant-ph].

[36] G. C. Wick, A. S. Wightman, and E. P. Wigner, The intrinsic parity of elementary particles, Phys. Rev. **88**, 101 (1952).

[37] G. C. Wick, A. S. Wightman, and E. P. Wigner, Superselection rule for charge, Phys. Rev. D **1**, 3267 (1970).

[38] S. D. Bartlett and H. M. Wiseman, Entanglement constrained by superselection rules, Phys. Rev. Lett. **91**, 097903 (2003).

[39] M.-C. Bañuls, J. I. Cirac, and M. M. Wolf, Entanglement in fermionic systems, Phys. Rev. A **76**, 022311 (2007).

[40] N. Friis, A. R. Lee, and D. E. Bruschi, Fermionic-mode entanglement in quantum information, Phys. Rev. A **87**, 022338 (2013).

[41] N. Friis, Reasonable fermionic quantum information theories require relativity, New Journal of Physics **18**, 033014 (2016).

[42] F. Benatti, R. Floreanini, F. Franchini, and U. Marzolino, Entanglement in indistinguishable particle systems, Physics Reports **878**, 1 (2020).

[43] N. T. Vidal, M. L. Bera, A. Riera, M. Lewenstein, and M. N. Bera, Quantum operations in an information theory for fermions, Phys. Rev. A **104**, 032411 (2021).

[44] R. Costa de Almeida and P. Hauke, From entanglement certification with quench dynamics to multipartite entanglement of interacting fermions, Phys. Rev. Res. **3**, L032051 (2021).

[45] T. Shen, H. Barghathi, A. D. Maestro, and B. Rubenstein, Disentangling the physics of the attractive Hubbard model via the accessible and symmetry-resolved entanglement entropies (2023), arXiv:2312.11746 [cond-mat.str-el].

[46] K. Ptaszyński and M. Esposito, Fermionic one-body entanglement as a thermodynamic resource, Phys. Rev. Lett. **130**, 150201 (2023).

[47] L. Ding, S. Mardazad, S. Das, S. Szalay, U. Schollwöck, Z. Zimborás, and C. Schilling, Concept of orbital entanglement and correlation in quantum chemistry, Journal of Chemical Theory and Computation **17**, 79 (2021), pMID: 33430597.

[48] An unpublished version of the implemented cluster extension can be found at https://doi.org/10.5281/zenodo.10628157.

[49] M. Capone, M. Civelli, S. S. Kancharla, C. Castellani, and G. Kotliar, Cluster-dynamical mean-field theory of the density-driven Mott transition in the one-dimensional Hubbard model, Phys. Rev. B **69**, 195105 (2004).

[50] E. Koch, G. Sangiovanni, and O. Gunnarsson, Sum rules and bath parametrization for quantum cluster theories, Phys. Rev. B **78**, 115102 (2008).

[51] C. Mejuto-Zaera, G. Weng, M. Romanova, S. J. Cotton, K. B. Whaley, N. M. Tubman, and V. Vlček, Are multi-quasiparticle interactions important in molecular ionization?, The Journal of Chemical Physics **154**, 121101 (2021).

[52] D. S. Levine, D. Hait, N. M. Tubman, S. Lehtola, K. B. Whaley, and M. Head-Gordon, CASSCF with extremely large active spaces using the adaptive sampling configuration interaction method, Journal of Chemical Theory and Computation **16**, 2340 (2020).

[53] C. Mejuto-Zaera, D. Tzeli, D. Williams-Young, N. M. Tubman, M. Matoušek, J. Brabec, L. Veis, S. S. Xantheas, and W. A. de Jong, The effect of geometry, spin, and orbital optimization in achieving accurate, correlated results for iron–sulfur cubanes, Journal of Chemical Theory and Computation **18**, 687 (2022).

[54] N. M. Tubman, J. Lee, T. Y. Takeshita, M. Head-Gordon, and K. B. Whaley, A deterministic alternative to the full configuration interaction quantum monte carlo method, The Journal of Chemical Physics **145**, 044112 (2016).

[55] D. B. Williams-Young, N. M. Tubman, C. Mejuto-Zaera, and W. A. de Jong, A parallel, distributed memory implementation of the adaptive sampling configuration interaction method, The Journal of Chemical Physics **158**, 214109 (2023).

[56] S. Bravyi and D. Gosset, Complexity of quantum impurity problems, Communications in Mathematical Physics **356**, 451 (2017).

[57] C. Mejuto-Zaera, L. Zepeda-Núñez, M. Lindsey, N. Tubman, B. Whaley, and L. Lin, Efficient hybridization fitting for dynamical mean-field theory via semi-definite relaxation, Phys. Rev. B **101**, 035143 (2020).

[58] G. Roósz, A. Kauch, F. Bippus, D. Wieser, and

K. Held, Two-site reduced density matrix from one- and two-particle Green's functions (2023), arXiv:2312.14275 [cond-mat.str-el].

[59] L. Stocker, S. H. Sack, M. S. Ferguson, and O. Zilberberg, Entanglement-based observables for quantum impurities, Phys. Rev. Res. **4**, 043177 (2022).

[60] C. Carisch and O. Zilberberg, Efficient separation of quantum from classical correlations for mixed states with a fixed charge, Quantum **7**, 954 (2023).

[61] E. H. Lieb and M. B. Ruskai, A fundamental property of quantum-mechanical entropy, Phys. Rev. Lett. **30**, 434 (1973).

[62] M. Tajik, I. Kukuljan, S. Sotiriadis, B. Rauer, T. Schweigler, F. Cataldini, J. Sabino, F. Moller, P. Schüttelkopf, S.-C. Ji, D. Sels, E. Demler, and J. Schmiedmayer, Verification of the area law of mutual information in a quantum field simulator, Nature Physics **19**, 1022 (2023).

[63] T. Schäfer, N. Wentzell, F. Šimkovic, Y.-Y. He, C. Hille, M. Klett, C. J. Eckhardt, B. Arzhang, V. Harkov, F. m. c.-M. Le Régent, A. Kirsch, Y. Wang, A. J. Kim, E. Kozik, E. A. Stepanov, A. Kauch, S. Andergassen, P. Hansmann, D. Rohe, Y. M. Vilk, J. P. F. LeBlanc, S. Zhang, A.-M. S. Tremblay, M. Ferrero, O. Parcollet, and A. Georges, Tracking the footprints of spin fluctuations: A multimethod, multimessenger study of the two-dimensional hubbard model, Phys. Rev. X **11**, 011058 (2021).

[64] M. Meixner, H. Menke, M. Klett, S. Heinzelmann, S. Andergassen, P. Hansmann, and T. Schäfer, Mott transition and pseudogap of the square-lattice hubbard model: results from center-focused cellular dynamical mean-field theory (2024), arXiv:2310.17302 [cond-mat.str-el].

[65] B.-X. Zheng, C.-M. Chung, P. Corboz, G. Ehlers, M.-P. Qin, R. M. Noack, H. Shi, S. R. White, S. Zhang, and G. K.-L. Chan, Stripe order in the underdoped region of the two-dimensional hubbard model, Science **358**, 1155–1160 (2017).

[66] A. Wietek, R. Rossi, F. Šimkovic, M. Klett, P. Hansmann, M. Ferrero, E. M. Stoudenmire, T. Schäfer, and A. Georges, Mott insulating states with competing orders in the triangular lattice hubbard model, Phys. Rev. X **11**, 041013 (2021).

[67] H. Xu, C.-M. Chung, M. Qin, U. Schollwöck, S. R. White, and S. Zhang, Coexistence of superconductivity with partially filled stripes in the hubbard model (2023), arXiv:2303.08376 [cond-mat.supr-con].

[68] M. Capone, M. Fabrizio, C. Castellani, and E. Tosatti, Strongly correlated superconductivity and pseudogap phase near a multiband Mott insulator, Phys. Rev. Lett. **93**, 047001 (2004).

[69] L. de' Medici, G. Giovannetti, and M. Capone, Selective Mott physics as a key to iron superconductors, Phys. Rev. Lett. **112**, 177001 (2014).

[70] P. Werner, S. Hoshino, and H. Shinaoka, Spin-freezing perspective on cuprates, Phys. Rev. B **94**, 245134 (2016).

[71] J. M. Tomczak, M. Van Schilfgaarde, and G. Kotliar, Many-body effects in iron pnictides and chalcogenides: Nonlocal versus dynamic origin of effective masses, Phys. Rev. Lett. **109**, 237010 (2012).

[72] A. Amaricci, J. C. Budich, M. Capone, B. Trauzettel, and G. Sangiovanni, First-order character and observable signatures of topological quantum phase transitions, Phys. Rev. Lett. **114**, 185701 (2015).

[73] L. Crippa, A. Amaricci, S. Adler, G. Sangiovanni, and M. Capone, Local versus nonlocal correlation effects in interacting quantum spin Hall insulators, Phys. Rev. B **104**, 235117 (2021).

[74] A. Richaud, M. Ferraretto, and M. Capone, Interaction-resistant metals in multicomponent fermi systems, Phys. Rev. B **103**, 205132 (2021).

[75] D. Tusi, L. Franchi, L. F. Livi, K. Baumann, D. Benedicto Orenes, L. Del Re, R. E. Barfknecht, T.-W. Zhou, M. Inguscio, G. Cappellini, M. Capone, J. Catani, and L. Fallani, Flavour-selective localization in interacting lattice fermions, Nature Physics **18**, 1201 (2022).

[76] A. Peres, Separability criterion for density matrices, Phys. Rev. Lett. **77**, 1413 (1996).

[77] P. Horodecki, Separability criterion and inseparable mixed states with positive partial transposition, Physics Letters A **232**, 333 (1997).

[78] R. Horodecki, P. Horodecki, M. Horodecki, and K. Horodecki, Quantum entanglement, Rev. Mod. Phys. **81**, 865 (2009).